Eur. Phys. J. C (2019) 79:177
https://doi.org/10.1140/epjc/s10052-019-6664-0

THE EUROPEAN PHYSICAL JOURNAL C

Regular Article - Theoretical Physics

Low-redshift constraints on the Hubble constant from the baryon acoustic oscillation "standard rulers" and the gravitational wave "standard sirens"

Zhe Chang[1,2], **Qing-Guo Huang**[2,3,4,5], **Sai Wang**[6,a], **Zhi-Chao Zhao**[1,2,b]

[1] Institute of High Energy Physics, Chinese Academy of Sciences, Beijing 100049, China
[2] School of Physical Sciences, University of Chinese Academy of Sciences, Beijing 100049, China
[3] CAS Key Laboratory of Theoretical Physics, Institute of Theoretical Physics, Chinese Academy of Sciences, Beijing 100190, China
[4] Center for Gravitation and Cosmology, College of Physical Science and Technology, Yangzhou University, Yangzhou 225009, China
[5] Synergetic Innovation Center for Quantum Effects and Applications, Hunan Normal University, Changsha 410081, China
[6] Department of Physics, The Chinese University of Hong Kong, Shatin, N.T., Hong Kong 999077, China

Received: 18 October 2018 / Accepted: 8 February 2019 / Published online: 26 February 2019

Abstract The multi-messenger observations of GW170817 indicated a new independent measurement of the Hubble constant (H_0). We obtain the low-redshift cosmological constraints on H_0 by combining this gravitational wave measurement with the observations of distance scales in baryon acoustic oscillations. Using Fisher information matrix, we estimate the projected constraints on H_0 from Einstein Telescope. Simulating 10^3 gravitational-wave standard sirens from binary neutron star coalescences, we find that Einstein Telescope alone can constrain H_0 almost as tightly as Planck final data release in the cosmological constant plus cold dark matter model. This constraint can be further improved by combining Einstein Telescope with Dark Energy Spectroscopic Instrument. The Hubble constant tension can thus be checked by observing the standard sirens with Einstein Telescope in the future.

1 Introduction

The recent observations of GW170817 [1] in both gravitational waves (GWs) and electromagnetic waves provide us a gravitational-wave "standard siren" measurement of the Hubble constant [2]. Advanced Laser Interferometer Gravitational-Wave Observatory (aLIGO) and Virgo can estimate the luminosity distance of GW170817 directly, and does not require any form of cosmic "distance ladder". In other words, the GW standard sirens are self-calibrated. Therefore, this is an independent measurement totally different from observations of the luminosity distance of Cepheids [3] and the cosmic microwave background (CMB) [4]. On the other hand, the electromagnetic wave analysis can infer the Hubble constant by measuring the recession velocity [2]. The Hubble's law says that the recession velocity is a product of H_0 and the proper distance. Therefore, the Hubble constant derived in this way is $H_0 = 70.0^{+12.0}_{-8.0}$ km s^{-1} Mpc^{-1} at 68% confidence level (CL) [2]. A recent work in Ref. [5] found a precise distance to the host galaxy of GW170817 and then shown $H_0 = 71.9 \pm 7.1$ km s^{-1} Mpc^{-1}. Ref. [6] obtained $H_0 = 69.9^{+4.7}_{-4.8}$ km s^{-1} Mpc^{-1} by combining the GW170817 and its electromagnetic (EM) counterpart GRB170817A with its radio counterpart.

The GW170817 constraints on H_0 are significantly less stringent than the pre-existing typical constraints, even though they are compatible with the latters. A local measurement of H_0, derived from the luminosity distances of Cepheids, shows $H_0 = 73.24 \pm 1.74$ km s^{-1} Mpc^{-1} at 68% CL [3]. The CMB constraint on H_0, obtained from a global fitting of the CMB data released by Planck 2015, gives $H_0 = 67.8 \pm 0.9$ km s^{-1} Mpc^{-1} at 68% CL [4]. Both constraints are much tighter than the GW constraint on H_0. However, the local measurement of H_0 is obviously in tension with the CMB constraint by more than 3σ. The former may be affected by residual systematics [7]. The latter relies on the assumption of cosmological models, for example, the spatially-flat base Λ Cold Dark Matter model (ΛCDM) model. Unfortunately, it is beyond the scope of the recent GW standard siren measurement to distinguish them from each other.

The GW170817 constraint on H_0 in Ref. [2] may bring underlying influences on the cosmological parameter infer-

[a] e-mail: wangsai@itp.ac.cn
[b] e-mail: zhaozc@ihep.ac.cn

ences. It can be viewed as a prior of H_0 in cosmological global fittings. A recent work in Ref. [8] combined it with the Planck 2015 observations of the CMB to explore a twelve-parameter extended ΛCDM scenario, and found that an inclusion of the recent GW prior of H_0 can significantly reduce the allowed parameter space.

As standard rulers, the distance scales measured in the baryon acoustic oscillation (BAO) can also be able to constrain H_0. In the ΛCDM model, for example, Ref. [9] determined H_0 with a 1.3% uncertainty using several BAO distance scales. Ref. [10] determined H_0 with a 3.38% uncertainty using several BAO distance scales including the recent anisotropic BAO measurements at nine effective redshift bins. Ref. [11] obtained $H_0 = 67.87^{+1.21}_{-1.86}$ km s^{-1} Mpc^{-1} by combining several BAO distance scales with the Alcock–Paczynski test.

In this work, we will study the constraints on the Hubble constant as well as other cosmological parameters by combining the GW170817 measurement of H_0 [2] with the measurements of distance scales in the BAO [12–15]. Both observations have relatively lower redshifts than the CMB. Beside the Hubble constant, we focus on the spatial curvature and the equation of state of the dark energy. Extending the parameter space can more or less reduce the dependence on cosmological models. We wonder if an inclusion of the recent GW standard siren measurement can significantly improve the constraints on these cosmological parameters. In addition, we will estimate the projected constraints on the cosmological parameters by combining the Einstein Telescope (ET) [16] with the Dark Energy Spectroscopic Instrument (DESI) project [17]. The technique of Fisher information matrix will be utilized for our estimation in this work. We expect that the two low-redshift cosmological observations can provide tighter constraints on the Hubble constant as well as other cosmological parameters in the future.

The rest of this paper is arranged as follows. Section 2 introduces the cosmological models and the data compilations. Section 3 presents the results of our parameter inferences. Section 4 demonstrates to what extent the luminosity distance can be measured by the ET. Section 5 shows the projected constraints on cosmological parameters from the ET and the DESI project. The conclusions and discussions are given in Sect. 6.

2 Cosmological models and data compilations

The Hubble constant is correlated with the spatial curvature and the equation of state of the dark energy. For a given value of the angular diameter distance to the last scattering surface, one can always adjust the values of the two parameters to compensate the variation of H_0 in principle. Using both BAO and GW data sets, we explore several extended cosmological models taking into account of the spatial curvature, or the equation of state of the dark energy, or both of them.

In the Friedmann–Lemaitre–Robertson–Walker Universe, the angular diameter distance $D_A(z)$ to an astrophysical object at redshift z is defined as

$$D_A(z) = \frac{1}{1+z} S_k\left(\int_0^z \frac{dz'}{H(z')}\right) , \tag{1}$$

where the function $S_k(x)$ is defined as

$$S_k(x) = \begin{cases} \frac{\sinh(H_0\sqrt{\Omega_k}x)}{H_0\sqrt{\Omega_k}} & (\Omega_k > 0), \\ x \quad (\Omega_k = 0), \\ \frac{\sin(H_0\sqrt{-\Omega_k}x)}{H_0\sqrt{-\Omega_k}} & (\Omega_k < 0), \end{cases} \tag{2}$$

and the Hubble parameter $H(z)$ is given by

$$H^2(z)/H_0^2 = \Omega_r(1+z)^4 + \Omega_m(1+z)^3 + \Omega_k(1+z)^2 + (1-\Omega_r-\Omega_m-\Omega_k) f(z) , \tag{3}$$

$$f(z) = \exp\left(\int_0^z 3(1+w(z'))\frac{dz'}{1+z'}\right), \tag{4}$$

where $w(z)$ denotes the equation of state of the dark energy. The parameters Ω_r, Ω_m, and Ω_k denote nowadays energy-density fractions of radiations, non-relativistic matter, and spatial curvature, respectively. To calculate the radiation density today, we refer to the formula $\Omega_r = \Omega_\gamma(1+0.2271 N_{\rm eff})$. We use the Planck best-fitting results, namely, the nowadays energy-density fraction of photons $\Omega_\gamma = 2.469 \times 10^{-5} h_0^{-2}$, and the relativistic degrees of freedom $N_{\rm eff} = 3.046$ [18,19]. Here we parameterize the Hubble constant as $H_0 = 100 h_0$ km s^{-1} Mpc^{-1}.

The sound horizon at the redshift z_d (the moment when the baryons decoupled from the Compton drag of the photons) can be calculated by using the Eisenstein and Hu formula [20]. It is given by

$$r_s(z_d) = \frac{1}{\sqrt{3}H_0}\int_0^{\frac{1}{1+z_d}} \frac{da}{a^2 E(a)\sqrt{1+\frac{3\Omega_b}{4\Omega_\gamma}a}} , \tag{5}$$

where z_d is given by a fitting formula, i.e. ,

$$z_d = \frac{1291(\Omega_m h_0^2)^{0.251}}{1+0.659(\Omega_m h_0^2)^{0.828}}\left(1+b_1(\Omega_b h_0^2)^{b_2}\right) , \tag{6}$$

$$b_1 = 0.313(\Omega_m h_0^2)^{-0.419}\left(1+0.607(\Omega_m h_0^2)^{0.674}\right) , \tag{7}$$

$$b_2 = 0.238(\Omega_m h_0^2)^{0.223} . \tag{8}$$

Here $a = 1/(1+z)$ denotes the scale factor of the Universe at redshift z. In this paper, we fix $\Omega_b h_0^2$ to its best-fit value obtained from Planck 2015 data release [4], namely, $\Omega_b h_0^2 =$

0.02222 ± 0.00023. The variations of $\Omega_b h_0^2$ within its error bar do not significantly shift our results.

The independent parameters which will be explored in this paper are composed of H_0, Ω_m, Ω_k, and the parameters in $w(z)$ parameterizations. To study the constraints on H_0, we introduce a single parameter to parameterize $w(z)$, and investigate the following models. First, we explore the parameter space $\{H_0,\ \Omega_m\}$ of the ΛCDM model. Second, we discuss the $\Omega_k\Lambda$CDM model with parameter space $\{H_0,\ \Omega_m,\ \Omega_k\}$. Third, we study the generic dark energy model, i.e., $w(z) = w$, which is a constant. This is called the wCDM model, and the parameter space is spanned by $\{H_0,\ \Omega_m,\ w\}$. Lastly, we consider the $\Omega_k w$CDM model, and the parameter space is $\{H_0,\ \Omega_m,\ \Omega_k,\ w\}$. We set priors as follows: $h_0 \in [0.4, 1]$, $\Omega_m \in [0.1, 0.9]$, $\Omega_k \in [-0.9, 0.9]$, and $w \in [-3.5, -0.5]$. All priors are uniform. To estimate the projected constraints on H_0 from future observations, we further consider the Chevallier–Polarski–Linder (CPL) parameterization [21,22]. In the CPL model, one assumes $w(z) = w_0 + w_a(1-a)$. Here w_0 and w_a are constants. Therefore, the parameter space is spanned by $\{H_0,\ \Omega_m,\ w_0,\ w_a\}$. If the parameter space is enlarged as $\{H_0,\ \Omega_m,\ \Omega_k,\ w_0,\ w_a\}$, the model is denoted as Ω_kCPL instead.

To explore the parameter space, we adopt the Cosmological Mente Carlo (CosmoMC) package [23], which is a publicly available Markov-Chain Monte-Carlo (MCMC) sampler for cosmological parameter inferences. We combine the GW170817 measurement of the Hubble constant [2] with the measurements of distance scales in the BAO [12–15]. Therefore, the adopted datasets include: the "BAO" which only includes the BAO measurements, and the "BAO+GW" which combines the BAO measurements and the GW170817 constraint on H_0.

For the measurements of distance scales in the BAO, we adopt the 6-degree Field Galaxy Survey [12], the Sloan Digital Sky Survey (SDSS) DR7 Main Galaxy Sample [13], the tomographic BAO analysis of the SDSS III Baryon Oscillation Spectroscopic Survey (BOSS) DR12 combined sample [14], and the SDSS IV extended Baryon Oscillation Spectroscopic Survey (eBOSS) DR14 quasar sample [15]. For the BOSS DR12 data, we use the tomographic nine effective redshift bins. For each bin, the anisotropic BAO estimators are given by $\frac{D_A(z)}{r_s(z_d)}$ and $H(z)r_s(z_d)$. For the other three data points, we refer to the isotropic BAO estimator which is defined as the volume-averaged effective distance, namely, $D_V(z) = (1+z)^{2/3} D_A^{2/3}(z) z^{1/3} H(z)^{-1/3}$.

For the GW170817 constraint on H_0 [2], we introduce a new likelihood of this data point into the CosmoMC package. Due to a highly non-Gaussian probability distribution function (PDF) of H_0 in GW170817, we explicitly utilize the PDF of H_0 shown in Fig. 1 of Ref. [2] as a H_0 prior in the CosmoMC.

3 The H_0 constraints from the GW170817 standard siren and the BAO standard rulers

For the four cosmological models, we list the 68% CL constraints on the independent parameters and the best-fit χ^2 in the Tables 1, 2, 3 and 4. We depict the one dimensional (1D) PDFs of the independent parameters and the two dimensional (2D) 68% and 95% CL contours of any two independent parameters in Figs. 1, 2, 3 and 4.

For the ΛCDM model, the 68% CL constraints on H_0 and Ω_m are shown in Table 1, and the 1D PDFs and the 2D contours are depicted in Fig. 1. As expected, the BAO only dataset reproduces the H_0 constraint in Ref. [10]. After the GW data is added, we do not find significant improvements to this constraint. Therefore, the BAO measurements dominate the constraints on cosmological parameters in the ΛCDM model.

For the $\Omega_k\Lambda$CDM model, the 68% CL constraints on H_0, Ω_m and Ω_k are shown in Table 2, and the 1D PDFs and the 2D contours are depicted in Fig. 2. Compared with the ΛCDM model, our cosmological constraints become not as tight as before due to an additional independent parameter Ω_k. The BAO data constrains the Hubble constant as 71^{+9}_{-20} km s^{-1} Mpc^{-1}, while the BAO+GW data constrains the Hubble constant as $73.1^{+5.2}_{-10.0}$ km s^{-1} Mpc^{-1}. The uncertainties on H_0 are reduced by around a half by adding the GW170817 data. We obtain similar results for the other two parameters. Therefore, the GW measurement, combining with the BAO distance measures, can significantly improve the constraints on cosmological parameters in the $\Omega_k\Lambda$CDM

Table 1 The 68% CL constraints on the independent parameters of the ΛCDM model

ΛCDM	BAO	BAO+GW
H_0	$69.6^{+2.1}_{-2.4}$	$69.6^{+2.0}_{-2.3}$
Ω_m	$0.324^{+0.034}_{-0.039}$	$0.324^{+0.032}_{-0.037}$
$\chi^2_{\rm min}$	20.2	26.3
$\frac{\chi^2_{\rm min}}{\rm DOF}$	1.06	1.32

Table 2 The 68% CL constraints on the independent parameters of the $\Omega_k\Lambda$CDM model

$\Omega_k\Lambda$CDM	BAO	BAO+GW
H_0	71^{+9}_{-20}	$73.1^{+5.2}_{-10.0}$
Ω_m	$0.318^{+0.14}_{-0.091}$	$0.343^{+0.049}_{-0.068}$
Ω_k	$0.01^{+0.16}_{-0.32}$	$-0.04^{+0.14}_{-0.10}$
$\chi^2_{\rm min}$	19.8	26.3
$\frac{\chi^2_{\rm min}}{\rm DOF}$	1.10	1.38

Table 3 The 68% CL constraints on the independent parameters of the wCDM model

wCDM	BAO	BAO+GW
H_0	82^{+20}_{-7}	$77.4^{+6.5}_{-11.0}$
Ω_m	$0.358^{+0.053}_{-0.034}$	0.348 ± 0.042
w	$-1.46^{+0.44}_{-0.40}$	$-1.27^{+0.38}_{-0.17}$
$\chi^2_{\min}$	19.8	26.2
$\frac{\chi^2_{\min}}{\mathrm{DOF}}$	1.10	1.38

Table 4 The 68% CL constraints on the independent parameters of the $\Omega_k w$CDM model

$\Omega_k w$CDM	BAO	BAO+GW
H_0	71^{+10}_{-20}	$73.1^{+5.2}_{-10.0}$
Ω_m	$0.272^{+0.088}_{-0.13}$	$0.294^{+0.064}_{-0.073}$
Ω_k	$0.18^{+0.22}_{-0.19}$	$0.13^{+0.18}_{-0.11}$
w	$-1.78^{+0.88}_{-0.39}$	$-1.82^{+0.91}_{-0.40}$
$\chi^2_{\min}$	19.3	25.6
$\frac{\chi^2_{\min}}{\mathrm{DOF}}$	1.14	1.42

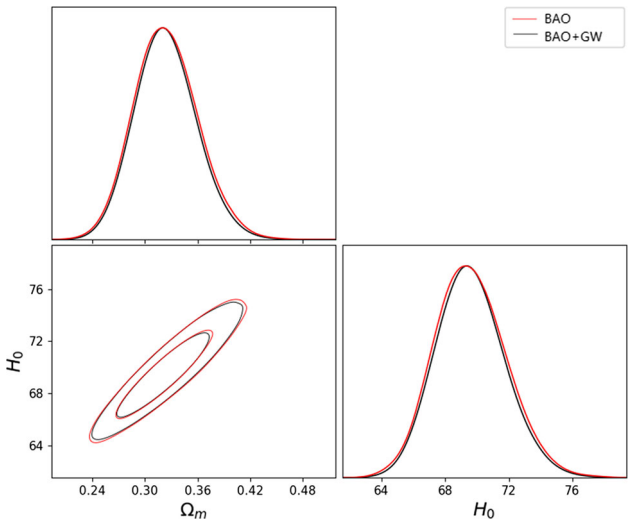

Fig. 1 The 1D PDFs and the 2D contours for the independent parameters in the ΛCDM model

model. In addition, the value of Ω_k is consistent with 0 within 68% CL.

For the wCDM model, the constraints on H_0, Ω_m and w are shown in Table 3, and the 1D PDFs and the 2D contours are depicted in Fig. 3. Compared with the ΛCDM model, the uncertainties become larger by around 30% for Ω_m, and by several times for H_0. The Hubble constant is constrained to be 82^{+20}_{-7} km s^{-1} Mpc^{-1} using the BAO data. After adding the GW data, it is improved to be $77.4^{+6.5}_{-11.0}$ km s^{-1} Mpc^{-1}. The constraint on H_0 is thus dominated by the GW data. The

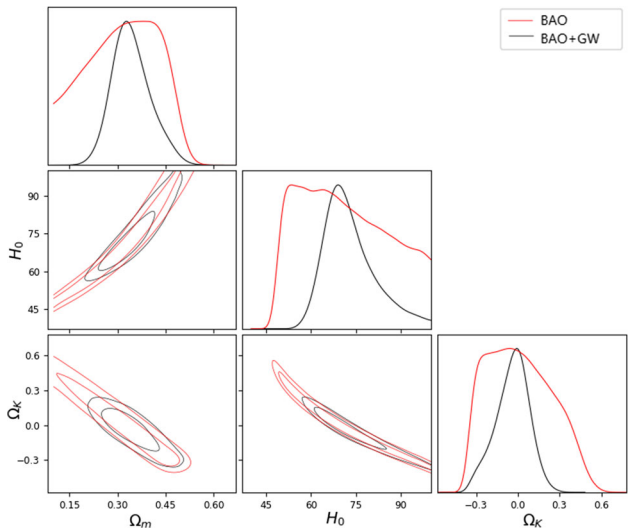

Fig. 2 The 1D PDFs and the 2D contours for the independent parameters in the $\Omega_k \Lambda$CDM model

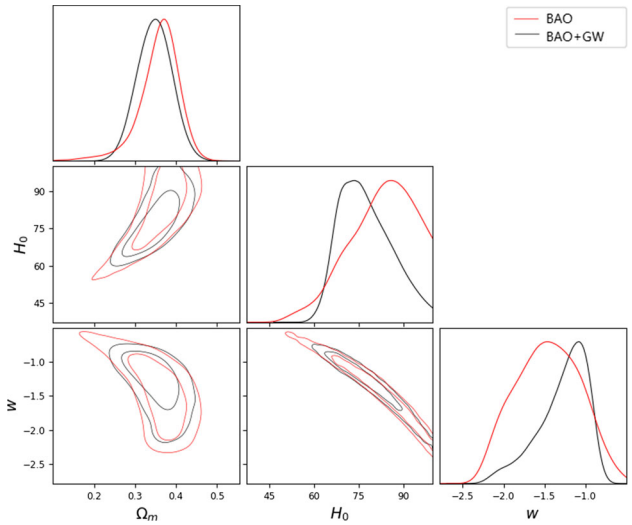

Fig. 3 The 1D PDFs and the 2D contours for the independent parameters in the wCDM model

constraints on two other parameters are also improved by adding the GW data. Therefore, the GW measurement, combining with the BAO distance measures, can significantly improve the cosmological constraints on the wCDM model. In addition, w is well consistent with the cosmological constant which takes $w = -1$.

For the $\Omega_k w$CDM model, the 68% CL constraints on H_0, Ω_m and w are shown in Table 4, and the 1D PDFs and the 2D contours are depicted in Fig. 4. The cosmological constraints become significantly looser than those in the former three models. The Hubble constant is constrained to be 71^{+10}_{-20} km s^{-1} Mpc^{-1} using the BAO data, while to be $73.1^{+5.2}_{-10.0}$ km s^{-1} Mpc^{-1} using the BAO+GW data. The uncertainty is reduced by a half by adding the GW170817

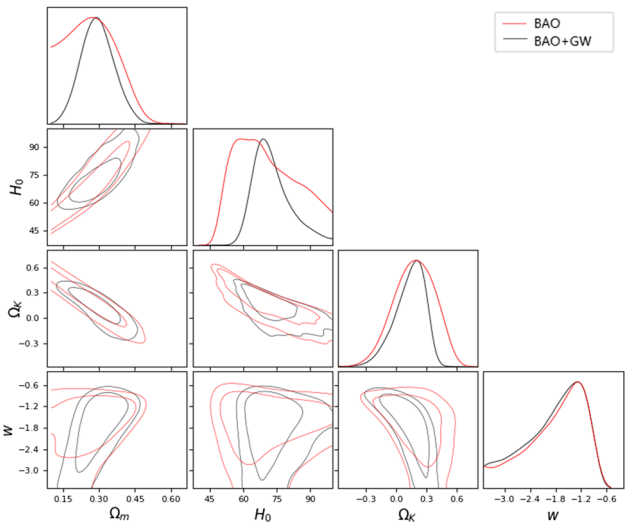

Fig. 4 The 1D PDFs and the 2D contours for the independent parameters in the $\Omega_k w$CDM model

data. For three other parameters, the constraints also become tighter after adding the GW170817 data. Therefore, the GW measurement, combining with the BAO distance measures, can significantly improve the constraints on cosmological parameters in the $\Omega_k w$CDM model. In addition, the value of Ω_k is well consistent with 0, and w is well consistent with -1.

In summary, the GW170817 measurement introduces little influence on the ΛCDM model. However, it dominates the cosmological constraints on H_0 and improves the constraints on other parameters for the three extended cosmological models which introduce the spatial curvature, or the generic dark energy, or both. In principle, we can also extend our studies to the CPL parameterization of dark energy. However, we find that the present data combinations can not provide tight constraints on w_a. In the following sections, we will show the projected constraints on w_a from future low-redshift observations. Our predictions will answer why we can not constrain w_a using the present data combinations.

4 Luminosity distance measured by Einstein Telescope

There is only a single GW standard siren which has been detected by the aLIGO and Virgo detectors. The H_0 constraint in Ref. [2] is expected to be improved if more and more GW standard sirens were captured in the future. A work shown that $\Delta H_0/H_0 \sim 0.042$ will be achieved after the third observational run of aLIGO and Virgo [24]. The ET [16], a third-generation ground-based GW detector, is designed with higher sensitivity than the second-generation aLIGO and Virgo. More GW standard sirens from binary neutron star coalescences are expected to be detected by the ET. In this section, we will demonstrate to what extent the luminosity distance of the GW sources can be measured by the ET in the future.

For a coalescence of a neutron binary, the waveform of GW in an inspiral stage can be written as a 3.5 post-Newtonian (PN) (i.e., at order $(v/c)^7$ beyond Newtonian gravity) formalism [25–33]. This formula includes the effect of gravitational radiation reaction. Over a single period, the change of orbital frequency is negligible. Therefore, the stationary phase approximation (SPA) can be employed to compute the waveform of GWs [34]. In the frequency domain, the waveform of GWs in the source frame is given by

$$\mathcal{H}(f) = \mathcal{A} f^{-7/6} \exp[i(2\pi f t_c + \pi/4 + \psi(f) - \varphi_{(2,0)})] \,, \tag{9}$$

where one takes the following expressions

$$\mathcal{A} = \sqrt{\frac{5}{96}} \frac{\mathcal{M}_c^{5/6}}{\pi^{2/3} d_L} \sqrt{[\mathcal{F}_+(1+\cos^2(\iota))]^2 + [\mathcal{F}_\times 2\cos(\iota)]^2} \,, \tag{10}$$

$$\psi(f) = \psi_c + \frac{3}{128\eta} \sum_{k=0}^{7} \psi_k (\pi M f)^{(k-5)/3} \,, \tag{11}$$

$$\varphi_{(2,0)} = \tan^{-1}\left(-\frac{2\cos(\iota)\mathcal{F}_\times}{(1+\cos^2(\iota))\mathcal{F}_+} \right) \,. \tag{12}$$

Here f is the GW frequency, d_L is a luminosity distance to the binary, t_c is a coalescence time, ψ_c is an orbital coalescence phase, and ι is an inclination angle between the line of sight and the orbital angular momentum of the binary. d_L can be written as

$$d_\mathrm{L} = (1+z)^2 D_\mathrm{A} \,. \tag{13}$$

A description of parameters ψ_k can be found in Ref. [35]. Conventionally, one represents the component masses m_1 and m_2 as a symmetric mass ratio $\eta = m_1 m_2/(m_1+m_2)^2$ and a chirp mass $\mathcal{M}_c = (m_1+m_2)\eta^{3/5}$. The total mass is thus given by $M = \mathcal{M}_c \eta^{-3/5}$. One should notice that the above formulae in Eqs. (9)–(12) are established in the source frame. However, the GWs would be detected in the observer frame. To transform to the observer frame, one should substitute m_i $(i = 1, 2)$ in the above formulae with $m_i(1+z)$, where z is a cosmological redshift of the GW source.

The antenna pattern functions $\mathcal{F}_{+,\times}$ in Eq. (10) describe the responses of an interferometer to a GW signal propagating from a polar angle θ and an azimuthal angle ϕ with a polarization angle ψ. As a possible design, the ET has three interferometers with opening angles of $\pi/3$ and 10 km length arms. Its antenna pattern functions are given by

$$\mathcal{F}_{+}^{(1)}(\theta,\phi,\psi)=\frac{\sqrt{3}}{2}\left[\frac{1}{2}(1+\cos^2(\theta))\cos(2\phi)\cos(2\psi)-\cos(\theta)\sin(2\phi)\sin(2\psi)\right], \tag{14}$$

$$\mathcal{F}_{\times}^{(1)}(\theta,\phi,\psi)=\frac{\sqrt{3}}{2}\left[\frac{1}{2}(1+\cos^2(\theta))\cos(2\phi)\sin(2\psi)+\cos(\theta)\sin(2\phi)\cos(2\psi)\right], \tag{15}$$

$$\mathcal{F}_{+,\times}^{(2)}(\theta,\phi,\psi)=\mathcal{F}_{+,\times}^{(1)}(\theta,\phi+2\pi/3,\psi), \tag{16}$$

$$\mathcal{F}_{+,\times}^{(3)}(\theta,\phi,\psi)=\mathcal{F}_{+,\times}^{(1)}(\theta,\phi+4\pi/3,\psi), \tag{17}$$

where the superscript $^{(a)}$ indicates the ath interferometer. The coefficient $\sqrt{3}/2$ arises from the $\pi/3$ opening angle of the ET [36,37].

In the frequency domain, the parameter space of the waveform is spanned by a set of nine independent parameters, namely, $\{\mathcal{M}_c,\ \eta,\ t_c,\ \psi_c,\ \iota,\ \psi,\ d_L,\ \theta,\ \phi\}$. However, the incident direction (θ,ϕ) of a GW standard siren can be exactly gotten by observing its electromagnetic counterpart. Therefore, a set of only seven independent parameters are left here. For the sake of simplicity, we denote them with $p_i=\{\ln\mathcal{M}_c,\ \ln\eta,\ t_c,\ \psi_c,\ \iota,\ \psi,\ \ln d_L\}$, where $i=1,2,3,\ldots,7$.

The capability of a GW detector to measure a GW signal is determined by its noise power spectral density (PSD). For all the three interferometers of the ET, we use the same PSD which is called ETB [38]. This PSD is expressed as

$$S_n(f)=10^{-50}\times(2.39\times10^{-27}x^{-15.64}+0.349x^{-2.145}+1.76x^{-0.12}+0.409x^{1.10})^2\mathrm{Hz}^{-1}\,. \tag{18}$$

where we define a dimensionless quantity $x=f/(100\mathrm{Hz})$.

The Fisher information matrix [34,39,40] is performed to estimate the projected constraints on cosmological parameters from future GW observations. For the a-th interferometer, the Fisher matrix is defined as

$$F_{ij}^{(a)}=\left\langle\frac{\partial\mathcal{H}^{(a)}(f)}{\partial p_i},\frac{\partial\mathcal{H}^{(a)}(f)}{\partial p_j}\right\rangle. \tag{19}$$

In the above definition, the angle bracket $\langle\rangle$ denotes a scalar product, i.e.

$$\langle h_1,h_2\rangle\equiv4\int_{f_{\mathrm{lower}}}^{f_{\mathrm{upper}}}\frac{h_1(f)h_2^*(f)+h_1^*(f)h_2(f)}{2S_n(f)}\mathrm{d}f\,, \tag{20}$$

where a superscript * denotes a conjugation. For the ET, we choose $f_{\mathrm{lower}}=1\mathrm{Hz}$, and S_n is essentially large for $f<1\mathrm{Hz}$. Following Ref. [36], we assume that the end of an inspiral regime occurs when its radiation frequency reaches $f_{\mathrm{upper}}=2f_{\mathrm{LSO}}$, where $f_{\mathrm{LSO}}=1/(6^{3/2}2\pi M_{\mathrm{obs}})$. Here $M_{\mathrm{obs}}=M(1+z)$ is the total mass in the observer frame. For multiple interferometers, the Fisher matrix is defined as follows

$$F=\sum_a F^{(a)}=F^{(1)}+F^{(2)}+F^{(3)}\,, \tag{21}$$

which is a summation of all the Fisher matrices for single interferometers. For the ET, the sum runs from 1 to 3 due to there being three interferometers in total. Therefore, we get the second equality in last equation.

We focus on the GW events which are generated by the mergers of the neutron star binaries. The short gamma-ray bursts will also be generated as the electromagnetic counterparts. They are believed to be highly beamed, since the gamma rays are emitted into a narrow cone which is almost perpendicular to the orbital plane of the inspiral. The inclination angle ι is thus narrow [41]. We assume it to satisfy a bimodal normal distribution within the range $[0^\circ,180^\circ]$, namely,

$$P(\iota)=\frac{1}{\sqrt{2\pi}\sigma}\times\begin{cases}\exp\left(-\frac{(\iota-\iota_0)^2}{2\sigma^2}\right)\\ \exp\left(-\frac{(\iota-\iota_\pi)^2}{2\sigma^2}\right)\end{cases}, \tag{22}$$

where we take $\iota_0=0^\circ$, $\iota_\pi=180^\circ$ and $\sigma=20^\circ$. This prior distribution of ι can be taken into account by adding an extra term to the Fisher matrix.[1] Therefore, we obtain the following transformation:

$$F_{ij}\longrightarrow F_{ij}+\frac{\delta_{ik}\delta_{jk}}{\sigma^2}\,, \tag{23}$$

where we take $k=5$ due to $\iota=p_5$. Without such a prior, the uncertainties on d_L and ι will be badly constrained because of a high degeneracy between them.

The root-mean-square (rms) uncertainty on the a-th parameter p_a is given by the a-th diagonal component of the covariance matrix C, i.e. $\Delta p_a=\sqrt{C_{aa}}$. The Cramer–Rao bound indicates an inequality of the form $C\geq F^{-1}$, where F is called Fisher matrix and F^{-1} means an inverse of F. Similar to a previous work [42], we employ the Cholesky decomposition to get the inverse matrix here. Therefore, a lower bound on the rms uncertainty of the i-th parameter is given by

$$\sigma_{p_i}=\sqrt{(F^{-1})_{ii}}\,. \tag{24}$$

Therefore, the projected constraints on any p_i can be inferred by calculating the Fisher matrix. In addition, a non-diagonal

[1] A method to add a Gaussian prior to Fisher matrix can be found via this link: http://www.stat.tamu.edu/~jlong/astrostat/fall2015/Fishermatrix.pdf.

element of $(F^{-1})_{ij}$ describes a correlation between p_i and p_j. Besides, we need to consider the effect of weak lensing on the luminosity distance. Similar to Ref. [43], we assume that the uncertainty due to weak lensing satisfies

$$\sigma_l = 0.05z\ . \tag{25}$$

Therefore, the total uncertainty on the luminosity distance is given by

$$\Delta \ln d_L = \sqrt{\sigma_o^2 + \sigma_l^2}, \tag{26}$$

where σ_o is given by σ_7 in Eq. (24) due to $\ln d_L = p_7$. The above discussion is available for a single GW event from the merger of neutron star binaries. In the next section, we will simulate multiple standard sirens to infer the constraints on the cosmological parameters.

5 Projected constraints on H_0 from ET and DESI

In this section, we will estimate the projected constraints on H_0 from future GW and BAO observations. As mentioned in last section, the ET has higher sensitivity than aLIGO and Virgo, and is expected to observe more standard sirens. On the other hand, the BAO distance measures are expected to be improved by the next-generation instruments of dark energy measurement, e.g. the DESI project [17]. Combining ET with DESI, we wonder if the constraint on H_0 can be improved significantly in the future. In this section, we explore six cosmological models, i.e. ΛCDM, $\Omega_k\Lambda$CDM, wCDM, $\Omega_k w$CDM, CPL, and Ω_kCPL. Note that the parameter w in $(\Omega_k)w$CDM is also written as w_0 here.

5.1 Constraints on H_0 from the ET

As mentioned in Sect. 1, the GW standard sirens are self-calibrated, implying that the luminosity distance can be measured without the necessity of any distance ladders. Meanwhile, their redshifts can be measured by observing the electromagnetic counterparts. Therefore, one can utilize the $d_L - z$ relation to infer the cosmological parameters. As mentioned in Sect. 2, we focus on the parameters $h_0,\ \Omega_m,\ \Omega_k,\ w_0,\ w_a$. Based on Planck 2015 data release [4], we set $h_0 = 0.673,\ \Omega_m = 0.313,\ \Omega_k = 0,\ w_0 = -1,\ w_a = 0$ as the fiducial model.

We utilize the Fisher information matrix to predict the uncertainties on H_0 and other cosmological parameters. For a set of multiple standard sirens, the Fisher matrix is defined as follows

$$F_{ij} = \sum_k \frac{\partial_i(\ln d_L(k))\partial_j(\ln d_L(k))}{(\Delta \ln d_L(k))^2}, \tag{27}$$

where both i and j run from 1 to 5, denoting the five independent parameters $\{w_0,\ w_a,\ \Omega_m,\ \Omega_k,\ h_0\}$ in order, and k denotes the k-th GW event located at $\{z_k,\ \hat{\gamma}_k\}$. Here z_k denotes the redshift of k-th event, and $\hat{\gamma}_k$ stands for a set of four angle parameters $\{\theta,\ \phi,\ \psi,\ \iota\}_k$. Not all of the binary neutron star coalescences are associated with electromagnetic counterparts. For the sources with $\iota < 20^\circ$ and $\iota > 160^\circ$, in this paper, we assume there being 10^3 GW standard sirens up to the redshift $z = 2$, at which the angle-averaged signal-to-noise ratio approximately reaches the value 8 [43].

Due to d_L being independent of $\hat{\gamma}$ and the event number being large, one can replace the sum over GW events in the above equation with an integral. Therefore, the following equation can be obtained [36]

$$F_{ij}^{GW} = \int_0^2 \partial_i(\ln d_L)\partial_j(\ln d_L) f(z) A(z) dz\ , \tag{28}$$

where $f(z)$ denotes the number distribution function of the GW standard sirens with respect to the redshift z, and $A(z)$ denotes an average of $(\Delta \ln d_L)^{-2}$ over a set of angle parameters $\{\theta,\ \phi,\ \psi,\ \iota\}$.

One can express the number distribution function of GW standard sirens as follows

$$f(z) = \frac{4\pi \mathcal{N} r(z) d_C^2(z)}{H(z)(1+z)}\ , \tag{29}$$

where $d_C = (1+z)D_A$ denotes a comoving distance, $r(z)$ is a source distribution function, and $\mathcal{N}$ is a constant ensuring the total number of the binary neutron star coalescences. Following Ref. [36], we consider a uniform distribution of $r(z)$, i.e. $r(z) = 1$, and a nonuniform distribution of it, i.e. $r(z) = 1 + 2z$ for $z \leq 1$, $r(z) = (15 - 3z)/4$ for $1 < z < 5$, and $r(z) = 0$ for otherwise. The nonuniform one is an approximation to the evolution of source rate suggested by Ref. [44]. In this work, the constant $\mathcal{N}$ is determined by requiring a relation of $\int_0^2 f(z)dz = 10^3$.

The Monte Carlo sampling method is utilized to obtain an expression for $A(z)$. We divide the redshift from 0 to 2 into 20 bins with a step 0.1. For each a bin, we generate 10^4 samples of $\{\theta, \phi, \psi, \iota\}$. Note that ι distributes following Eq. (22), while the three others are uniform. The mass of a neutrino star is set as $m_{\rm NS} = 1.4M_\odot$. Averaging $(\Delta \ln d_L)^{-2}$ over 10^4 samples of $\{\theta, \phi, \psi, \iota\}$ for each redshift bin, we show our results with red dots in Fig. 5. We also fit our results with the following formula:

$$A^{-1/2}(z) = 0.009295z^3 - 0.04530z^2 + 0.1398z + 0.01941, \tag{30}$$

which is shown with blue solid curve in Fig. 5. In addition, we have checked our method by reproducing the results of

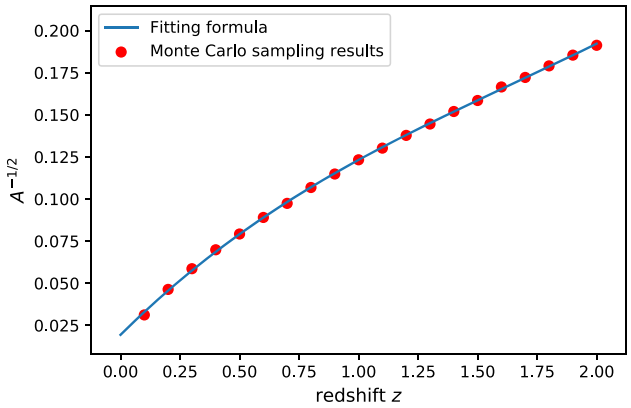

Fig. 5 The fitting formula $A^{-1/2}(z)$ as a function of redshift z. The red dots arise from the Monte Carlo simulation, while the blue solid curve denotes a fitting formula in Eq. (30)

Ref. [45] with the code developed by us. Finally, we substitute Eq. (30) into Eq. (28) to calculate the Fisher matrix of cosmological parameters. Our detailed results will be shown in the following.

For the five parameters explored here, their GW Fisher matrices are shown as 5×5 matrices in Tables 5 and 6 for the cases with uniform and nonuniform distributions, respectively. There is a specific set of cosmological parameters for a given cosmological model. To obtain the 1σ uncertainties on these parameters, one can construct a Fisher matrix associated with these parameters by marginalizing the original Fisher matrix over other remaining parameters. For example, if the ΛCDM model is considered, one should construct a Fisher matrix associated with Ω_m and h_0 by marginalizing the 5×5 Fisher matrix over w_0, w_a and Ω_k. In other words, one removes the 1st, 2nd, and 4th columns and rows from the two matrices in Tables 5 and 6, respectively, and the remaining items thus form the required Fisher matrices for the ΛCDM model. A similar approach works for other cosmological models.

Once the Fisher matrix is gotten for a given cosmological model, as mentioned in last section, one can infer the 1σ uncertainties on the corresponding cosmological parameters by finding its inverse matrix. For the cases of uniform and nonuniform distributions, our results are shown in Tables 7 and 8, respectively. The constraints on H_0 and other parameters are a little tighter for the uniform distribution than those for the nonuniform distribution. The reason is that the GW sources are more concentrated at $z = 1$ in the nonuniform distribution, and thus there are less sources at both higher and lower redshifts. Comparing with the uniform distribution, therefore, it is difficult for the nonuniform distribution to trace the evolution of the dark energy.

For the ΛCDM model, the 1σ uncertainties on the independent parameters Ω_m and h_0 are listed in the first rows of Tables 7 and 8. For the cases of uniform and nonuniform distributions, we find that the ET alone can achieve sensitivities of $\Delta H_0 = 0.5953\,\mathrm{km\,s^{-1}\,Mpc^{-1}}$ and $\Delta H_0 = 0.7245\,\mathrm{km\,s^{-1}\,Mpc^{-1}}$, respectively. Both constraints are tighter than the one from Planck 2015 data release. Our results show that the ET GW observations may provide new insights to checking the tension between the local measurement of H_0 and the global fitting of Planck CMB.

For the $\Omega_k\Lambda$CDM model, the 1σ uncertainties on Ω_m, Ω_k and h_0 are listed in the second rows of Tables 7 and 8. For the cases of uniform and nonuniform distributions, we find that the ET can achieve sensitivities of $\Delta H_0 = 0.7654\,\mathrm{km\,s^{-1}\,Mpc^{-1}}$ and $\Delta H_0 = 0.9609\,\mathrm{km\,s^{-1}\,Mpc^{-1}}$, respectively. Comparing with Planck 2015 results, we find that the ET can still get tighter constraints on H_0 even in the $\Omega_k\Lambda$CDM model when the GW sources distribute uniformly.

Table 5 The ET GW Fisher matrix for the uniform distribution of GW sources

	w_0	w_a	Ω_m	Ω_k	h_0
w_0	2.095×10^3	3.526×10^2	6.401×10^3	4.365×10^3	1.824×10^4
w_a	3.526×10^2	6.319×10^1	1.139×10^3	7.801×10^2	2.926×10^3
Ω_m	6.401×10^3	1.139×10^3	2.062×10^4	1.412×10^4	5.381×10^4
Ω_k	4.365×10^3	7.801×10^2	1.412×10^4	9.678×10^3	3.664×10^4
h_0	1.824×10^4	2.926×10^3	5.381×10^4	3.664×10^4	1.687×10^5

Table 6 The ET GW Fisher matrix for the nonuniform distribution of GW sources

	w_0	w_a	Ω_m	Ω_k	h_0
w_0	2.053×10^3	3.558×10^2	6.402×10^3	4.368×10^3	1.733×10^4
w_a	3.558×10^2	6.474×10^1	1.161×10^3	7.948×10^2	2.905×10^3
Ω_m	6.402×10^3	1.161×10^3	2.088×10^4	1.430×10^4	5.270×10^4
Ω_k	4.368×10^3	7.948×10^2	1.430×10^4	9.798×10^3	3.591×10^4
h_0	1.733×10^4	2.905×10^3	5.270×10^4	3.591×10^4	1.521×10^5

Table 7 Projected constraints on cosmological parameters from the ET GWs for the uniform distribution of GW sources

GW uniform	Δw_0	Δw_a	$\Delta\Omega_m$	$\Delta\Omega_k$	Δh_0
ΛCDM	–	–	1.703×10^{-2}	–	5.953×10^{-3}
$\Omega_k\Lambda$CDM	–	–	4.343×10^{-1}	6.153×10^{-1}	7.654×10^{-3}
wCDM	1.992×10^{-1}	–	3.771×10^{-2}	–	1.233×10^{-2}
$\Omega_k w$CDM	4.451×10^{-1}	–	1.038	1.375	1.642×10^{-2}
CPL	2.969×10^{-1}	3.637	1.836×10^{-1}	–	2.185×10^{-2}
Ω_kCPL	6.585×10^{-1}	1.128×10^{-1}	3.747	4.263	2.917×10^{-2}

Table 8 Projected constraints on cosmological parameters from the ET GWs for the nonuniform distribution of GW sources

GW nonuniform	Δw_0	Δw_a	$\Delta\Omega_m$	$\Delta\Omega_k$	Δh_0
ΛCDM	–	–	1.955×10^{-2}	–	7.245×10^{-3}
$\Omega_k\Lambda$CDM	–	–	4.666×10^{-1}	6.574×10^{-1}	9.609×10^{-3}
wCDM	2.324×10^{-1}	–	4.041×10^{-2}	–	1.596×10^{-2}
$\Omega_k w$CDM	5.326×10^{-1}	–	1.142	1.507	2.180×10^{-2}
CPL	3.889×10^{-1}	4.258	2.074×10^{-1}	–	2.939×10^{-2}
Ω_kCPL	6.978×10^{-1}	1.345×10^{-1}	4.220	4.759	3.993×10^{-2}

For the wCDM model, the 1σ uncertainties on Ω_m, w and h_0 are listed in the third rows of Tables 7 and 8. For the cases of uniform and nonuniform distributions, we find that the ET can achieve sensitivities of $\Delta H_0 = 1.233\,\mathrm{km\,s^{-1}\,Mpc^{-1}}$ and $\Delta H_0 = 1.596\,\mathrm{km\,s^{-1}\,Mpc^{-1}}$, respectively. Both constraints are not as tight as Planck 2015 results. However, they are still tighter than the local measurement of H_0 derived from the luminosity distances of Cepheids.

In the $\Omega_k w$CDM model, the 1σ uncertainties on Ω_m, Ω_k, w and h_0 are listed in the forth rows of Tables 7 and 8. For the cases of uniform and nonuniform distributions, we find that the ET can achieve sensitivities of $\Delta H_0 = 1.642\,\mathrm{km\,s^{-1}\,Mpc^{-1}}$ and $\Delta H_0 = 2.180\,\mathrm{km\,s^{-1}\,Mpc^{-1}}$, respectively. The former is almost comparable to the local measurement of H_0, while the latter is less stringent.

For other cosmological models, i.e. CPL and Ω_kCPL, we show our predicted constraints on H_0 in the last three rows of Tables 7 and 8, respectively. The 1σ uncertainties on H_0 are obviously larger than that of the local measurement of H_0. The reason is that there is an extra dependent parameter in the equation of state of the dark energy. In addition, for the CPL model, we find $\Delta w_a = 3.637$ and $\Delta w_a = 4.258$ for the cases of uniform and nonuniform distributions, respectively. For the Ω_kCPL model, we find both uncertainties being about three times larger. These are reasons why we do not use the existing datasets to constrain w_a in Sect. 3.

Furthermore, we can obtain the correlations among the five cosmological parameters by using the non-diagonal elements of the inverse of Fisher matrix. For example, the 68% CL correlations between H_0 and other parameters are depicted as the two-dimensional contours in Fig. 6. Here the black curves denote the uniform distribution of GW sources, while the blue curves denote the nonuniform source distribution of GW sources. We find that H_0 is anti-correlated with four other parameters.

5.2 Combine ET with the DESI project

As mentioned in Sect. 2, the BAO standard rulers depend on the angular diameter distance $D_A(z)$ and the Hubble parameter $H(z)$, both of which rely on the five parameters $\{h_0,\ \Omega_m, \Omega_k,\ w_0,\ w_a\}$. The property of the dark energy can be determined by measuring these two quantities at different redshift bins. To explore the detection ability of the BAO method, we employ the Fisher matrix to analyze the sensitivity of a typical experiment, e.g. the DESI project.

For the BAO method, the Fisher information matrix is constructed as follows [46]

$$F_{ij}^{BAO} = \sum_z \frac{\partial_i(\ln D_A(z))\partial_j(\ln D_A(z))}{(\Delta\ln D_A(z))^2} + \sum_z \frac{\partial_i(\ln H(z))\partial_j(\ln H(z))}{(\Delta\ln H(z))^2} \tag{31}$$

where the sum runs over all of the redshift bins z. Here $\Delta\ln D_A(z)$ and $\Delta\ln H(z)$ denote the 1σ uncertainties on $\ln D_A(z)$ and $\ln H(z)$, respectively. For DESI, which covers a redshift range from 0.6 to 1.9 with an area of 14,000 deg^2, they can be found in Table 2.3 of Ref. [17].[2]

Calculating the above formula numerically, we obtain all the elements of the DESI BAO Fisher matrix, which are listed

[2] In Ref. [17], the fiducial model is given by Planck 2013 results. In this work, our fiducial model is given by Planck 2015 results. However, the effects due to the difference between both models are negligible for our forecasts.

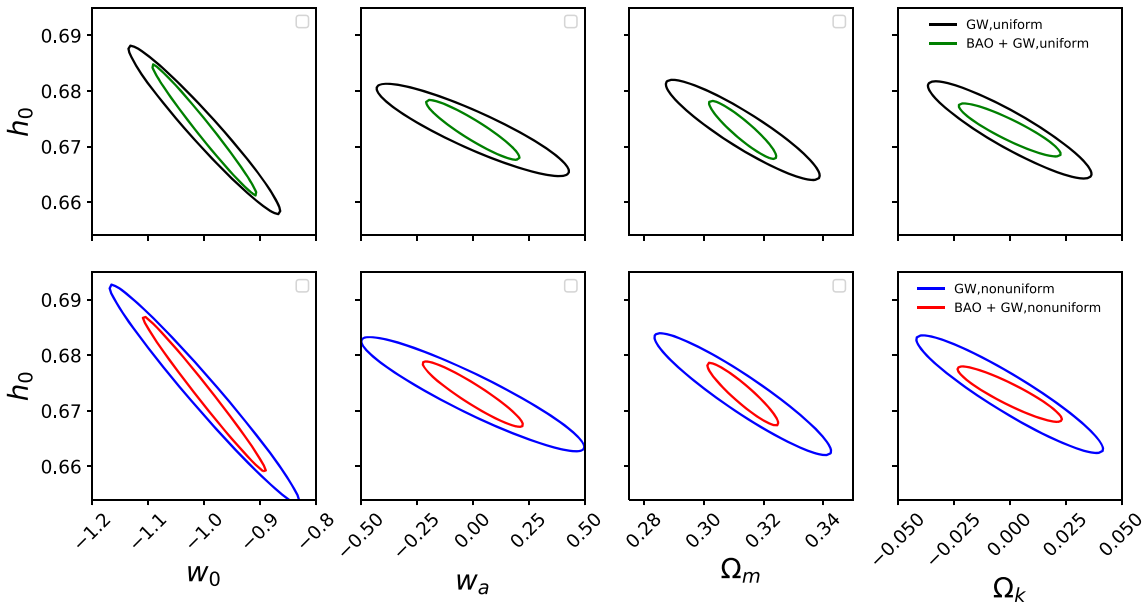

Fig. 6 The 2D contours between h_0 and w_0, w_a, Ω_m, Ω_k at 68% CL. The upper/lower panels denote the uniform/nonuniform distribution of GW sources. The black and blue curves refer to the ET, while the green and red ones refer to the combinations of ET and DESI

Table 9 The DESI BAO Fisher matrix

	w_0	w_a	Ω_m	Ω_k	h_0
w_0	6.537×10^3	1.356×10^3	2.395×10^4	9.054×10^3	4.939×10^4
w_a	1.356×10^3	3.001×10^2	5.366×10^3	2.050×10^3	1.010×10^4
Ω_m	2.395×10^4	5.366×10^3	9.677×10^4	3.680×10^4	1.793×10^5
Ω_k	9.054×10^3	2.050×10^3	3.680×10^4	1.442×10^4	6.704×10^4
h_0	4.939×10^4	1.010×10^4	1.793×10^5	6.704×10^4	3.773×10^5

Table 10 Projected constraints on cosmological parameters from the DESI BAOs

BAO	Δw_0	Δw_a	$\Delta\Omega_m$	$\Delta\Omega_k$	Δh_0
ΛCDM	–	–	9.289×10^{-3}	–	4.704×10^{-3}
$\Omega_k\Lambda$CDM	–	–	2.318×10^{-2}	4.978×10^{-2}	4.867×10^{-3}
wCDM	1.378×10^{-1}	–	1.093×10^{-2}	–	1.601×10^{-2}
$\Omega_k w$CDM	1.595×10^{-1}	–	2.388×10^{-2}	5.760×10^{-2}	1.907×10^{-2}
CPL	7.186×10^{-1}	3.733	1.535×10^{-1}	–	6.707×10^{-2}
Ω_kCPL	7.303×10^{-1}	3.742	1.568×10^{-1}	5.774×10^{-2}	6.872×10^{-2}

in Table 9. Similar to what we did in the last subsection, we can obtain the projected constraints on all the six cosmological models from the DESI BAOs only. We list our results in Table 10. For any cosmological model considered here, the 1σ uncertainty on H_0 is smaller than the one in Planck 2015 results.

To obtain a joint constraint on H_0 from DESI and ET, we can obtain a joint Fisher matrix by adding together the DESI BAO Fisher matrix and the ET GW Fisher matrix. For the cases of uniform and nonuniform distributions, respectively, we can obtain the joint Fisher matrices by using Tables 5, 9 and Tables 6, 9. Then we obtain Tables 11 and 12 for the projected constraints on all the six cosmological models. Similar to what we did in last subsection, we can infer the projected constraints on the six cosmological models using the two Fisher matrices. We will demonstrate our detailed results in the following.

For the ΛCDM model, the 1σ uncertainties on the independent parameters Ω_m and h_0 are listed in the first rows of Tables 11 and 12. For the cases of uniform and nonuniform distributions, we find that the ET alone can achieve sensitivities of $\Delta H_0 = 0.3468$ km s^{-1} Mpc^{-1} and $\Delta H_0 = 0.3727$ km s^{-1} Mpc^{-1}, respectively. Both constraints are tighter than the one from Planck 2015 data release. Our

Table 11 Projected constraints on cosmological parameters from the combination of DESI BAOs and ET GWs for the uniform distribution of GW sources

BAO + GW uniform	Δw_0	Δw_a	$\Delta\Omega_m$	$\Delta\Omega_k$	Δh_0
ΛCDM	–	–	7.479×10^{-3}	–	3.468×10^{-3}
$\Omega_k\Lambda$CDM	–	–	1.130×10^{-2}	2.273×10^{-2}	3.538×10^{-3}
wCDM	8.630×10^{-2}	–	1.034×10^{-2}	–	8.388×10^{-3}
$\Omega_k w$CDM	8.642×10^{-2}	–	1.314×10^{-2}	2.277×10^{-2}	8.394×10^{-3}
CPL	1.902×10^{-1}	1.362	5.880×10^{-2}	–	1.564×10^{-2}
Ω_kCPL	1.903×10^{-1}	1.364	5.905×10^{-2}	2.279×10^{-2}	1.567×10^{-2}

Table 12 Projected constraints on cosmological parameters from the combination of DESI BAOs and ET GWs for the nonuniform distribution of GW sources

GW nonuniform + BAO	Δw_0	Δw_a	$\Delta\Omega_m$	$\Delta\Omega_k$	Δh_0
ΛCDM	–	–	7.906×10^{-3}	–	3.727×10^{-3}
$\Omega_k\Lambda$CDM	–	–	1.157×10^{-2}	2.257×10^{-2}	3.790×10^{-3}
wCDM	9.761×10^{-2}	–	1.044×10^{-2}	–	1.003×10^{-2}
$\Omega_k w$CDM	9.782×10^{-2}	–	1.316×10^{-2}	2.262×10^{-2}	1.003×10^{-2}
CPL	2.413×10^{-1}	1.581	6.720×10^{-2}	–	2.065×10^{-2}
Ω_kCPL	2.414×10^{-1}	1.584	6.733×10^{-2}	2.266×10^{-2}	2.068×10^{-2}

results show that the ET GW observations combining with BAO observations can provide new insights to checking the Hubble constant tension.

For the $\Omega_k\Lambda$CDM model, the 1σ uncertainties on Ω_m, Ω_k and h_0 are listed in the second rows of Tables 11 and 12, For the cases of uniform and nonuniform distributions, we find that the ET can achieve sensitivities of $\Delta H_0 = 0.3538$ km s^{-1} Mpc^{-1} and $\Delta H_0 = 0.3790$ km s^{-1} Mpc^{-1}, respectively. Comparing with Planck 2015 results, we find that the ET and BAO can get tighter constraints on H_0.

For the wCDM model, the 1σ uncertainties on Ω_m, w and h_0 are listed in the third rows of Tables 11 and 12. For the cases of uniform and nonuniform distributions, we find that the ET can achieve sensitivities of $\Delta H_0 = 0.8388$ km s^{-1} Mpc^{-1} and $\Delta H_0 = 1.003$ km s^{-1} Mpc^{-1}, respectively. Both constraints are almost as tight as Planck 2015 results.

In the $\Omega_k w$CDM model, the 1σ uncertainties on Ω_m, Ω_k, w and h_0 are listed in the forth rows of Tables 11 and 12. For the cases of uniform and nonuniform distributions, we find that the ET can achieve sensitivities of $\Delta H_0 = 0.8394$ km s^{-1} Mpc^{-1} and $\Delta H_0 = 1.003$ km s^{-1} Mpc^{-1}, respectively. The former is almost comparable to the local measurement of H_0, while the latter is less stringent.

For other cosmological models, i.e. CPL and Ω_kCPL, we show our predicted constraints on H_0 in the last three rows of Tables 11 and 12, respectively. For the uniform distribution of GW sources, the 1σ uncertainty on H_0 is obviously smaller than that of the local measurement of H_0, while for the nonuniform one it is obviously lager. In addition, for the CPL model, we find $\Delta w_a = 1.362$ and $\Delta w_a = 1.581$ for the uniform and nonuniform distributions of GW sources, respectively. For the Ω_kCPL model, they become $\Delta w_a = 1.364$ and $\Delta w_a = 1.584$, respectively. Therefore, we may be able to tightly constrain H_0 in dark energy models by combining ET with DESI in the future.

For the joint analysis of ET and DESI, the 68% CL correlations between H_0 and other parameters are also depicted as the two-dimensional contours in Fig. 6. Here the green curves denote the uniform distribution of GW sources, while the red curves denote the nonuniform source distribution of GW sources. We find that H_0 is still anti-correlated with four other parameters.

6 Conclusion and discussion

In this work, we obtained low-redshift cosmological constraints on the Hubble constant by combining the GW170817 standard siren with several BAO standard rulers. We found that the GW170817 brings little influence on the H_0 constraint in the ΛCDM model, while it is significant when additional cosmological parameters, i.e. Ω_k and w, are considered. The present data combinations can not be used to test the Hubble constant tension, due to significantly large uncertainties on H_0. The uncertainty on H_0 is expected to be reduced by observing more GW standard sirens.

Using Fisher information matrix, we estimated the projected constraints on H_0 from the ET by simulating 10^3 GW standard sirens from the binary neutron star coalescences.

In the ΛCDM model, we found that the ET alone can constrain H_0 tighter than the Planck 2015 results. The Hubble constant tension can thus be checked by the ET in the future. However, this constraint was significantly weakened if other cosmological parameters, i.e. Ω_k, w_0 and w_a, were included. Combining DESI BAOs with ET GWs together can significantly reduce the uncertainties on H_0, even in dark energy models.

After the writing of this paper, we notice that Planck Collaboration makes public its final data release [47]. The updated constraint on the Hubble constant is shown as $H_0 = 67.4 \pm 0.5$ km s^{-1} Mpc^{-1} at 68% CL. Assuming 10^3 GW standard sirens from the binary neutron star coalescences, therefore, we can use the ET to obtain slightly less stringent constraints on H_0 than that of Planck final data release. Therefore, more than $\simeq 10^3$ GW standard sirens are of necessity for the ET to obtain a H_0 constraint as tight as Planck final data release. However, we can still obtain more stringent constraints on H_0 by combining the DESI BAO distance measures with the ET's 10^3 GW standard sirens.

Acknowledgements Z. C. and Z.-C. Z are supported by Grants from NSFC (Grant 11675182 and 11690022). Q.-G. H. is supported by Grants from NSFC (Grant no. 11335012, 11575271, 11690021, 11747601), Top-Notch Young Talents Program of China, and partly supported by the Strategic Priority Research Program of CAS and Key Research Program of Frontier Sciences of CAS. We would like to appreciate Dr. Yuting Wang for providing us the tomographic BAO data of the SDSS III BOSS DR12 combined sample in Ref. [14]. S. W. is indebted to Prof. Wen Zhao for helpful discussions on Fisher matrix and gravitational-wave standard sirens. Z.-C. Z. greatly appreciate Dr. Atsushi Nishizawa and Dr. Yu Sang for useful discussions.

Data Availability Statement This manuscript has no associated data or the data will not be deposited. [Authors' comment: The data used in this paper can be downloaded in other's paper (e.g. References [2] and [12–15]).]

Funded by SCOAP^3.

References

1. B. P. Abbott et al., [Virgo, LIGO Scientific Collaborations], Phys. Rev. Lett. **119**, 161101 (2017). arXiv:1710.05832
2. B. P. Abbott et al., [LIGO Scientific, Las Cumbres, VINROUGE, DES, DLT40, Virgo, 1M2H, MASTER, DEC], Nature (2017). arXiv:1710.05835
3. A.G. Riess et al., Astrophys. J. **826**, 56 (2016). arXiv:1604.01424
4. P. A. R. Ade et al., [Planck Collaboration], Astron. Astrophys. **594**, A13 (2016). arXiv:1502.01589
5. M. Cantiello et al., Astrophys. J. **854**, L31 (2018). arXiv:1801.06080
6. K. Hotokezaka, E. Nakar, O. Gottlieb, S. Nissanke, K. Masuda, G. Hallinan, K. P. Mooley, A. Deller, (2018). arXiv:1806.10596
7. G. Efstathiou, Mon. Not. R. Astron. Soc. **440**, 1138 (2014). arXiv:1311.3461
8. E. Di Valentino, A. Melchiorri, Phys. Rev. D **97**, 041301 (2018). arXiv:1710.06370
9. C. Cheng, Q.-G. Huang, Sci. China Phys. Mech. Astron. **58**, 599801 (2015). arXiv:1409.6119
10. Y. Wang, L. Xu, G.-B. Zhao, Astrophys. J. **849**, 84 (2017). arXiv:1706.09149
11. X. Zhang, Q.-G. Huang, X.-D. Li, (2018). arXiv:1801.07403
12. F. Beutler, C. Blake, M. Colless, D.H. Jones, L. Staveley-Smith, L. Campbell, Q. Parker, W. Saunders, F. Watson, Mon. Not. R. Astron. Soc. **416**, 3017 (2011). arXiv:1106.3366
13. A.J. Ross, L. Samushia, C. Howlett, W.J. Percival, A. Burden, M. Manera, Mon. Not. R. Astron. Soc. **449**, 835 (2015). arXiv:1409.3242
14. G.-B. Zhao et al., [BOSS], Mon. Not. R. Astron. Soc. **466**, 762 (2017). arXiv:1607.03153
15. M. Ata et al., Mon. Not. R. Astron. Soc. (2017). arXiv:1705.06373
16. M. Punturo, Class. Quantum Gravity **27**, 194002 (2010)
17. A. Aghamousa et al., [DESI] (2016). arXiv:1611.00036
18. L.A. Popa, A. Vasile, JCAP **0806**, 028 (2008). arXiv:0804.2971
19. G. Mangano, G. Miele, S. Pastor, M. Peloso, Phys. Lett. B **534**, 8 (2002). arXiv:astro-ph/0111408
20. D.J. Eisenstein, W. Hu, Astrophys. J. **496**, 605 (1998). arXiv:astro-ph/9709112
21. M. Chevallier, D. Polarski, Int. J. Mod. Phys. D **10**, 213 (2001). arXiv:gr-qc/0009008
22. E.V. Linder, Phys. Rev. Lett. **90**, 091301 (2003). arXiv:astro-ph/0208512
23. A. Lewis, S. Bridle, Phys. Rev. D **66**, 103511 (2002). arXiv:astro-ph/0205436
24. N. Seto, K. Kyutoku, Mon. Not. R. Astron. Soc. **475**, 4133 (2018). arXiv:1710.06424
25. Y. Itoh, Class. Quantum Gravity **21**, S529 (2004). arXiv:gr-qc/0401059
26. L. Blanchet, B.R. Iyer, Phys. Rev. D **71**, 024004 (2005). arXiv:gr-qc/0409094
27. L. Blanchet, T. Damour, G. Esposito-Farese, B.R. Iyer, Phys. Rev. Lett. **93**, 091101 (2004). arXiv:gr-qc/0406012
28. L. Blanchet, T. Damour, G. Esposito-Farese, Phys. Rev. D **69**, 124007 (2004). arXiv:gr-qc/0311052
29. Y. Itoh, T. Futamase, Phys. Rev. D **68**, 121501 (2003). arXiv:gr-qc/0310028
30. Y. Itoh, Phys. Rev. D **69**, 064018 (2004). arXiv:gr-qc/0310029
31. L. Blanchet, G. Faye, B. R. Iyer, and B. Joguet, Phys. Rev. D **65**, 061501 (2002). [Erratum: Phys. Rev.D71,129902(2005)], arXiv:gr-qc/0105099
32. Y. Itoh, T. Futamase, H. Asada, Phys. Rev. D **63**, 064038 (2001). arXiv:gr-qc/0101114
33. T. Damour, P. Jaranowski, G. Schaefer, Phys. Lett. B **513**, 147 (2001). arXiv:gr-qc/0105038
34. C. Cutler, E.E. Flanagan, Phys. Rev. D **49**, 2658 (1994). arXiv:gr-qc/9402014
35. B.S. Sathyaprakash, B.F. Schutz, Living Rev. Relativ. **12**, 2 (2009). arXiv:0903.0338
36. W. Zhao, C. van den Broeck, D. Baskaran, T.G.F. Li, Phys. Rev. D **83**, 023005 (2011). arXiv:1009.0206
37. T. G. F. Li, Doctoral thesis, Vrije U., Amsterdam (2013). http://inspirehep.net/record/1266133/files/thesis_T_G_F_Li.pdf. Accessed Dec 2017
38. T. Regimbau et al., Phys. Rev. D **86**, 122001 (2012). arXiv:1201.3563
39. L.S. Finn, D.F. Chernoff, Phys. Rev. D **47**, 2198 (1993). arXiv:gr-qc/9301003

40. E. Poisson, C.M. Will, Phys. Rev. D **52**, 848 (1995). arXiv:gr-qc/9502040
41. N. Dalal, D.E. Holz, S.A. Hughes, B. Jain, Phys. Rev. D **74**, 063006 (2006). arXiv:astro-ph/0601275
42. S. Wang (2017). arXiv:1712.06072
43. B.S. Sathyaprakash, B.F. Schutz, C. Van Den Broeck, Class. Quantum Gravity **27**, 215006 (2010). arXiv:0906.4151
44. R. Schneider, V. Ferrari, S. Matarrese, S. F. Portegies Zwart, Mon. Not. R. Astron. Soc. **324**, 797 (2001). arXiv:astro-ph/0002055
45. A. Nishizawa, A. Taruya, S. Saito, Phys. Rev. D **83**, 084045 (2011). arXiv:1011.5000
46. A. Albrecht et al., (2006). arXiv:astro-ph/0609591
47. N. Aghanim et al., [Planck Collaboration], Planck 2018 results. VI. Cosmological parameters. arXiv:1807.06209 [astro-ph.CO]